

Dalton Transactions

Accepted Manuscript

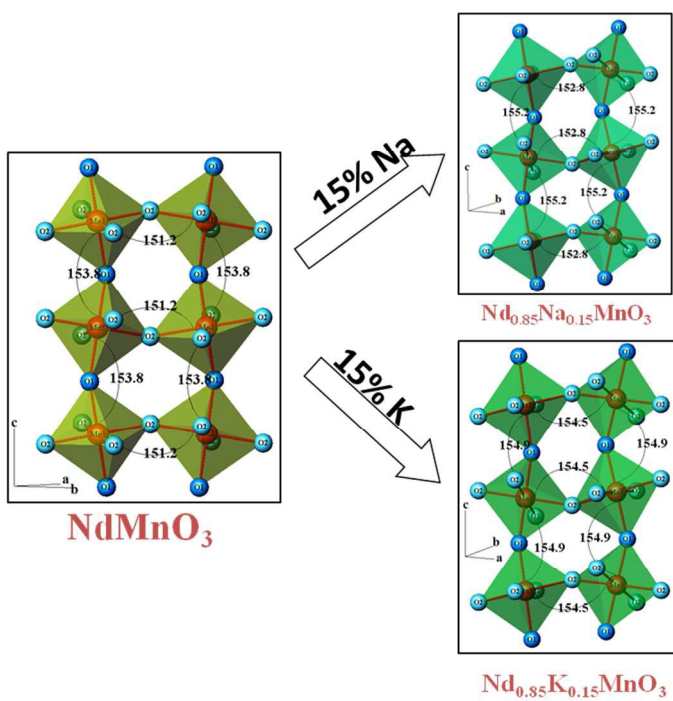


This is an *Accepted Manuscript*, which has been through the Royal Society of Chemistry peer review process and has been accepted for publication.

Accepted Manuscripts are published online shortly after acceptance, before technical editing, formatting and proof reading. Using this free service, authors can make their results available to the community, in citable form, before we publish the edited article. We will replace this *Accepted Manuscript* with the edited and formatted *Advance Article* as soon as it is available.

You can find more information about *Accepted Manuscripts* in the [Information for Authors](#).

Please note that technical editing may introduce minor changes to the text and/or graphics, which may alter content. The journal's standard [Terms & Conditions](#) and the [Ethical guidelines](#) still apply. In no event shall the Royal Society of Chemistry be held responsible for any errors or omissions in this *Accepted Manuscript* or any consequences arising from the use of any information it contains.



15% monovalent Sodium and Potassium doping reduces the structural distortion of NdMnO₃ with a subsequent modification in magnetic behavior.

Effect of monovalent cation doping on structure, microstructure, lattice distortion and magnetic behavior of single crystalline NdMnO₃ compound

Anshuman Nandy, S. K. Pradhan *

Materials Science Division, Department of Physics, The University of Burdwan,

West Bengal-713104, India

* Corresponding author, e-mail: skpradhan@phys.buruniv.ac.in, Telephone: +91-342-2657800

Abstract

Pure and 15mol% Na, K-doped NdMnO₃ compounds with perovskite structure are prepared by sol-gel method. Tiny single crystals are formed after sintering the compounds at 1000°C. Effect of Na and K doping as well as effect of sintering temperature on formation and microstructure of NdMnO₃ are studied in details by Rietveld refinement technique using X-ray powder diffraction data. Single phase formation and single crystalline growth is also confirmed by high resolution transmission electron microscopy (HRTEM). Bond angles and bond lengths are calculated and shown by 3D diagrams. Monovalent doping induces noticeable changes in the microstructure and yields better structural stability in these compounds. Doping results in change of Mn-O, Nd-O and Mn-O-Mn bond lengths which in turn reduce the lattice and octahedral distortion in the system along with an increase in tolerance factor. Magnetic properties of these compounds are also modified as a result of doping. Temperature dependent magnetization results show that Neel temperature of antiferromagnetic NdMnO₃ compound is 67.2K and the Curie temperatures of ferromagnetic Nd_{0.85}Na_{0.15}MnO₃ and Nd_{0.85}K_{0.15}MnO₃ compounds are 99.1K and 98.6K respectively. Both 15% Na and K doping results in a similar T_C in doped NdMnO₃ compounds.

Introduction

Perovskite structured ABO_3 type rare earth manganates are well known and explored extensively for their novel magnetic and electronic transport properties and important applications in industries.¹⁻⁸ Some important features of these compounds include temperature dependent magnetization, Colossal magnetoresistance, charge ordering, metal-insulator transition etc.¹⁻⁸ These properties arise from some complex interplay between spin, charge and orbital ordering and lattice deformations of these compounds.⁹⁻¹⁰ The structural and microstructural parameters of these compounds impart significant role on their properties.¹⁻⁶ The basic building block of $RMnO_3$ (R=rare earth) perovskite structure is MnO_6 octahedra. The structural deformation of perovskite lattice mainly occurs from two types of distortions: (i) tilting of MnO_6 octahedra which arises from the mismatch of ionic radii of R and Mn and (ii) lattice distortion which originates from the Jahn-Teller effect due to length asymmetry in six Mn-O bonds surrounding the Mn atom in MnO_6 octahedra.⁶ The degree of lattice distortion can be measured by Goldschmidt tolerance factor (t).¹¹ For an ideal cubic perovskite structure, $t = 1$ and Mn-O-Mn bond is straight (bond angle = 180°). When lattice distortion is introduced in the structure, t becomes less than 1 and Mn-O-Mn bond angles become less than 180° . Doping by a monovalent or divalent cation at R site changes the degree of ionic size mismatch as well as the Mn-O bond length and Mn-O-Mn bond angle and thus modifies the lattice distortions arising from both the tilting of octahedra and Jahn-Teller effect. A detailed discussion on structure and lattice distortion of $RMnO_3$ perovskite manganites was reported by Alonso et al.¹² The microstructure and the octahedral distortion influence the behavior of these compounds to a great extent and this distortion can be changed significantly by doping at R site. The effects of different divalent cation doping in place of R site on improving lattice and octahedral distortions and their role on

the magnetic and electronic transport properties of the compounds were reported in details.¹⁻⁶ However, the structural and microstructural distortion in RMnO₃ compounds due to monovalent doping at R site is yet to be studied in details. To study the structural distortion and modification of structure due to same amount monovalent dopants with different ionic radii, we consider NdMnO₃, Nd_{0.85}K_{0.15}MnO₃ and Nd_{0.85}Na_{0.15}MnO₃. Comprehensive magnetic structure and magnetic properties of undoped and divalent doped NdMnO₃ compounds were well characterized by several authors.¹³⁻²³ Among several rare earth perovskites, Nd-based system shows a larger lattice distortion originating from smaller Nd atoms.¹⁵ However, the in depth structural characterization and study of monovalent cation doping effect on octahedral distortion were not addressed previously.²⁴⁻²⁸ NdMnO₃ shows a paramagnetic to antiferromagnetic phase transition with Neel temperature at 67K.²⁹ On the other hand, both 15mol% Na- and K-doped NdMnO₃ compounds show paramagnetic to ferromagnetic phase transition with Curie temperature at ~100K.²⁵⁻²⁹ In this article emphasis is given on the following aspects: (i) detailed crystal structures, microstructures and lattice distortions in these three compounds due to monovalent doping, (ii) effect of sintering temperature on the formation of these compounds and (iii) temperature dependent magnetization to elucidate the effect of monovalent doping on the magnetic properties of NdMnO₃.

Experimental

Pure undoped and 15 mol% K- and Na- doped NdMnO₃ compounds were prepared by sol-gel route. The oxide precursors were transformed to a colloidal solution of respective nitrates and dried to obtain a homogeneous gel. For pure compound, neodymium oxide (Nd₂O₃) (purity, >99%, SRL) and manganese (II) acetate tetrahydrate ((CH₃COO)₂Mn.4H₂O) (purity, >99.5%, MERCK) powder precursors were taken in stoichiometric ratio and transformed to respective

nitrate solutions [Nd(NO₃)₃ and Mn(NO₃)₃] by adding small amount of conc. HNO₃ to powder precursors. The nitrate solution was then boiled to remove excess HNO₃. An equivalent amount of citric acid and later on few drops of ethylene glycol was added to the mixture and stirred for 3h. After homogeneous mixing, the mixture was kept at 80°C for 10h to obtain a homogeneous gel. The gel was fired at 200°C and the obtained powder was then finely crushed and sintered in open air at 500°C and 800°C each for 6h duration with an intermediate furnace cooling to room temperature. A part of the sample sintered at 800°C was taken out for experiments and rest of the powder was finally sintered at 1000°C for 10h. To prepare Nd_{0.85}K_{0.15}MnO₃ and Nd_{0.85}Na_{0.15}MnO₃ compounds, 15mol% of Nd₂O₃ was replaced by equivalent amount of potassium carbonate (K₂CO₃, purity, MERCK) and sodium carbonate (Na₂CO₃, purity, MERCK) respectively. Similar preparation methods were followed for these compounds and powders sintered at 800°C and 1000°C were collected for experiments. This is so far, one of the fastest preparation methods for these compounds.

Structural and microstructural characterizations of the undoped and 15 mol% K- and Na-doped NdMnO₃ compounds were done by XRD and HRTEM. XRD patterns of sintered samples were recorded with D8 Advanced diffractometer (Bruker, Da Vinci model) using CuK_α radiation in step scan mode (step size: 0.02°, counting time: 2sec/step) for the angular range 20°-80° 2θ. For HRTEM study, a pinch of powder was dispersed ultrasonically in ethyl alcohol and a drop of the colloidal solution was placed on carbon coated Cu grid. The structure, microstructure and morphology of particles were studied from the images of HRTEM (JEOL-JEM 2010), operated at 200 KV. The dc magnetization values at low temperatures were recorded by a quantum design Superconducting Quantum Interference Device (SQUID) magnetometer in the 30K-300K temperature range.

Method of analysis

Structural and microstructural characterizations of the prepared compounds are performed by analyzing the XRD patterns of these compounds employing Rietveld powder structure refinement method^{30, 31} using MAUD software (version 2.26).^{32, 33} Both the structural and microstructure parameters are refined through Marquardt least-squares method. The peak shape is assumed to be a pseudo-Voigt function as it takes care for both the particle size and strain broadening of the experimental profiles. The structural parameters, such as lattice parameters, atomic coordinates, atomic occupancies, oxygen vacancy etc and microstructure parameters such as particle size and r.m.s. lattice strain of all three compounds are obtained from the Rietveld refinement. The background of each pattern is fitted by a polynomial of degree five. The observed X-ray powder diffraction patterns of these compounds are fitted by refining several structural and microstructural parameters of the simulated XRD patterns generated considering the simultaneous presence of all pertinent phases from their respective ICSD database. Initially, positions of all peaks are corrected by successive refinements of zero-shift error. Considering the integrated intensity of the peaks as a function of structural and microstructural parameters, the Marquardt least-squares procedure is adopted for minimizing the difference between the observed and simulated powder diffraction patterns and the minimization is monitored using the reliability index parameter, R_{wp} (weighted residual error) and R_{exp} (expected error) defined, respectively, as

$$R_{wp} = \left[\frac{\sum_i w_i (I_0 - I_c)^2}{\sum_i w_i (I_0)^2} \right]^{1/2}$$

$$R_{\text{exp}} = \left[\frac{(N - P)}{\sum_i w_i (I_0)^2} \right]^{1/2}$$

where I_0 and I_C are the experimental and calculated intensities, w_i ($=1/I_0$) and N are the weight and number of experimental observations and P the number of fitting parameters. This leads to the value of goodness of fit (GoF):

$$\text{GoF} = \frac{R_{\text{wp}}}{R_{\text{exp}}}$$

Refinements of all parameters are performed until convergence is reached with the value of the quality factor, GoF very close to 1.0 (varies between 1.2 and 1.4 for the present case), which confirms the goodness of refinement. Microstructure parameters such as particle size, lattice strain values of sintered samples are obtained from this analysis along with all structural parameters. Caglioti parameters U , V , W , instrumental asymmetry and Gaussianity parameters are obtained for the instrumental setup using a specially prepared Si standard and kept fixed during refinements. HRTEM images are analyzed using ImageJ software and the average distance between the planes were measured. Some structural models are prepared using ATOM software (version 6).

Results and discussion

Structural Characterization by XRD

The undoped and 15% Na, K doped NdMnO_3 compounds are sintered at 800°C and then at 1000°C temperature to obtain the single phase stoichiometric compounds in tiny single crystalline form. The light brown color powders of all these compounds transform to dark brown after sintering at 800°C and finally turn into black after sintering at 1000°C . Typical Rietveld

refined outputs of XRD patterns of undoped and doped NdMnO_3 compounds sintered at 800°C in open air each for

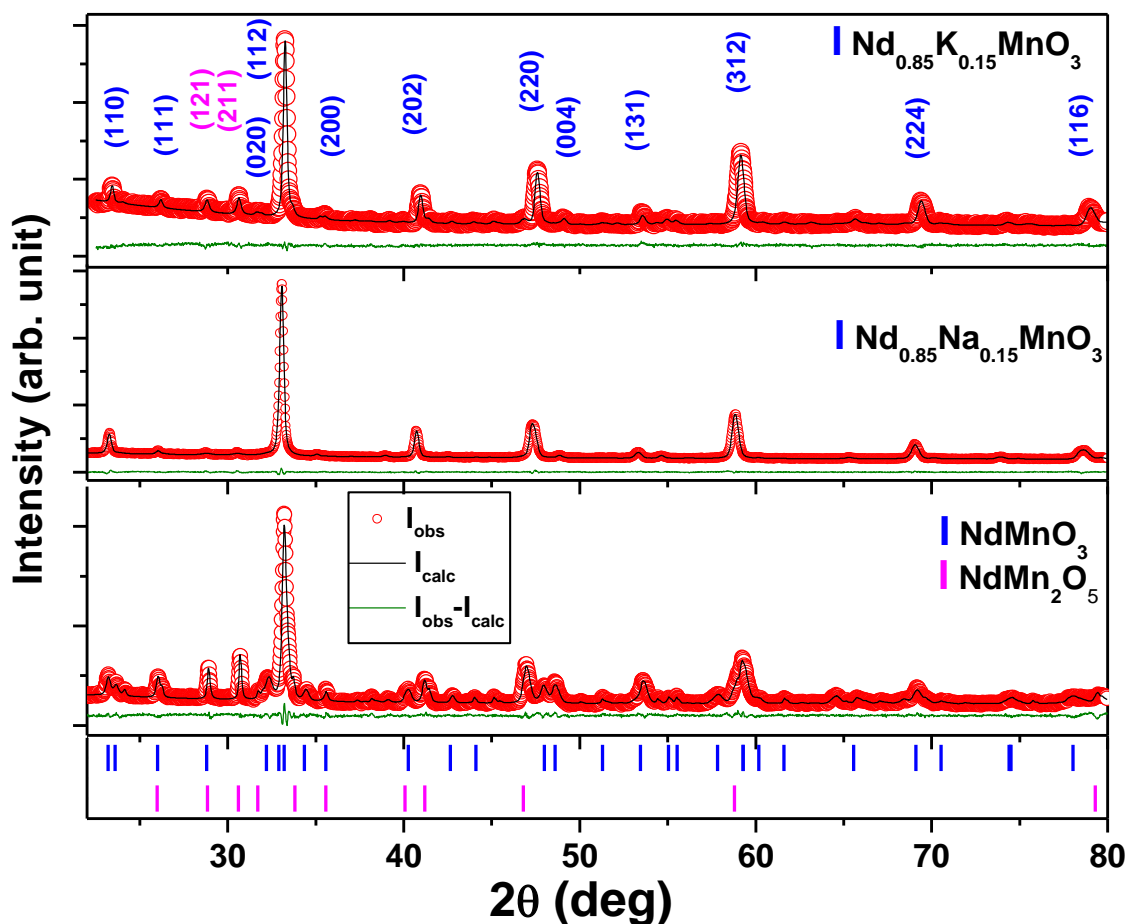


Fig. 1 Experimental (o) and Rietveld refined (-) XRD patterns of undoped, Na- and K- doped NdMnO_3 powders sintered at 800°C for 6 h. Peak positions are marked (l) at the bottom of the respective patterns.

6h duration is shown in Figure 1. Refined patterns are shown by black continuous lines through the experimental data points, represented by small red circles. The residue between observed and calculated ($I_{\text{o}}-I_{\text{c}}$) patterns is shown at the bottom of respective patterns. All compounds belong to

same orthorhombic phase (ICSD code # 93624, space group: P_{bnm} , $a=5.4397\text{\AA}$, $b=5.6247\text{\AA}$, $c=7.6351\text{\AA}$).³⁴ It may be noted that in all three compounds two reflections (121) and (211) at $\sim 28.0^\circ$ and $\sim 31.0^\circ$ 2θ do not belong to these compounds but to an intermediate orthorhombic NdMn_2O_5 phase (ICSD code# 91768, space group: P_{bam} , $a=7.4970\text{\AA}$, $b=8.6086\text{\AA}$, $c=5.6963\text{\AA}$). Microstructural parameters and relative phase abundances of NdMnO_3 and NdMn_2O_5 phases in all three compounds are revealed from Rietveld analysis and tabulated in Table 1. Crystallite sizes and r.m.s. lattice strains in all three compounds are found to be isotropic in nature.

Table 1: Microstructural parameters and relative phase abundances of NdMnO_3 and NdMn_2O_5 phases in samples sintered at 800°C for 6h.

Sample	Lattice Parameters (\AA)			Crystallite Size (nm)	R.m.s. Strain ($\times 10^{-3}$)
	a	b	c		
Undoped NdMnO_3 NdMnO_3 : 71.8 mol% NdMn_2O_5 : 28.2 mol%	5.4192(8)	5.6004(8)	7.6414(0)	70.24(3)	1.6(4)
$\text{Nd}_{0.85}\text{Na}_{0.15}\text{MnO}_3$ $\text{Nd}_{0.85}\text{Na}_{0.15}\text{MnO}_3$: 90.1 mol% NdMn_2O_5 : 9.9 mol%	5.4605(0)	5.4651(3)	7.7005(5)	76.32(1)	1.46(2)
$\text{Nd}_{0.85}\text{K}_{0.15}\text{MnO}_3$ $\text{Nd}_{0.85}\text{K}_{0.15}\text{MnO}_3$: 75.98 mol% NdMn_2O_5 : 24.02 mol%	5.4293(4)	5.4440(2)	7.6708(1)	105.33(5)	0.953(4)

In none of these samples composition of the major phase is stoichiometric due to the presence of significant amount of secondary NdMn_2O_5 phase. Results suggest that Na- doping is more effective in obtaining a single major phase. However, it seems that 800°C sintering temperature is not sufficient to obtain a single phase with accurate stoichiometric compositions of these compounds. Among three compounds, crystallite size in undoped compound is less due to inherent distortion. It is evident that in case of doped compounds, $\mathbf{a} \approx \mathbf{b}$. Thus, the doped lattices are more symmetrical and less distorted and as a result crystallite (coherently diffracting domain) sizes are bigger in these two compounds. However, r.m.s. lattice strains in all three compounds are significantly present due to the presence of secondary phase and reduces to a small extent after doping with K- and Na.

The Rietveld refined XRD powder patterns of undoped, 15mol% Na- and K- doped NdMnO_3 powders sintered at 1000°C are shown in Figure 2. It is interesting to note that all three compounds completely transformed to a single orthorhombic phase and there is no trace of secondary NdMn_2O_5 phase in all three XRD patterns. It suggests that all three compounds become perfectly stoichiometric after sintering at 1000°C for 10h. XRD patterns of undoped, Na- and K- doped and NdMnO_3 compounds are fitted very well with the same orthorhombic phase used for 800°C sintered powders.

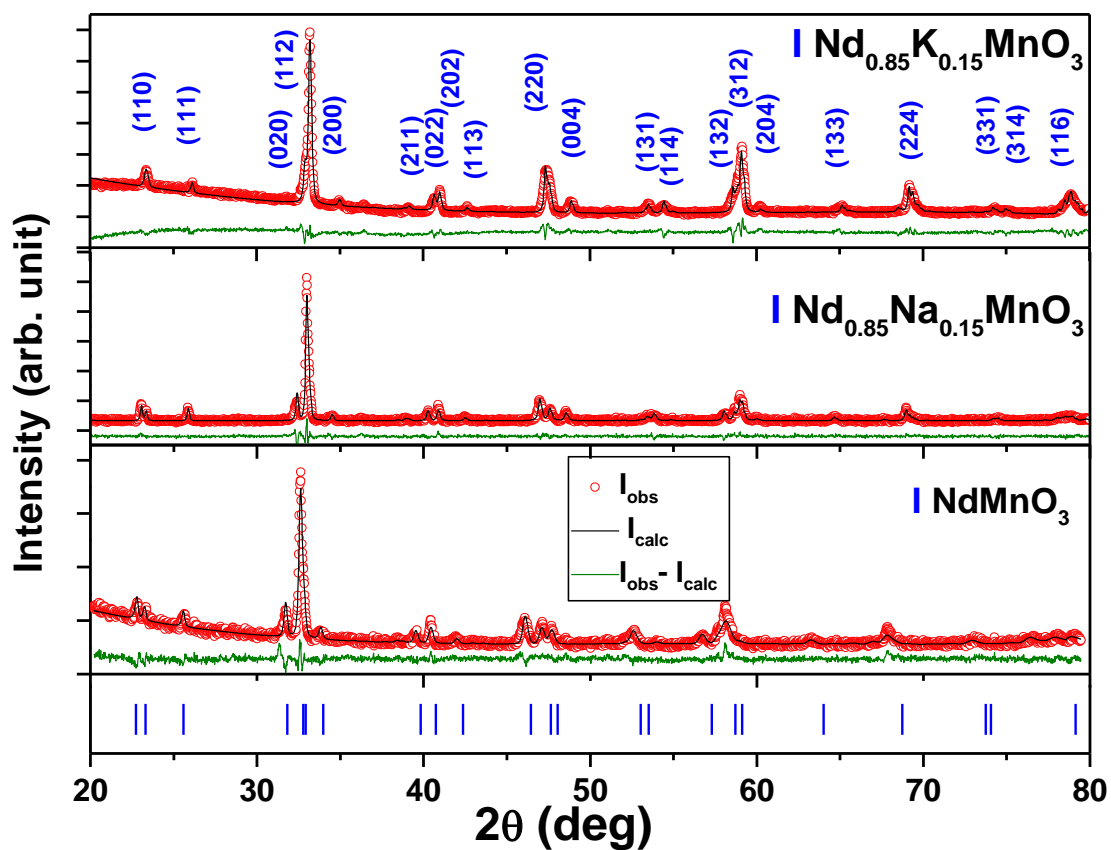


Fig. 2 Experimental (o) and Rietveld refined (-) XRD patterns of undoped, Na- and K- doped NdMnO_3 powders sintered at 1000°C for 10 h. Peak positions are marked (|) at the bottom of the respective patterns.

Table 2: Structural and microstructure parameters of undoped and 15mol% K- and Na- doped NdMnO₃ compounds sintered at 1000°C for 10 h.

Compound →	NdMnO ₃	Nd _{0.85} Na _{0.15} MnO ₃	Nd _{0.85} K _{0.15} MnO ₃
Goodness of Fit	1.37	1.25	1.35
Space Group	P _{bnm}	P _{bnm}	P _{bnm}
a (Å)	5.5183(9)	5.4249(0)	5.4299(5)
b (Å)	5.7058(3)	5.5470(1)	5.4936(7)
c (Å)	7.7725(4)	7.6636(0)	7.6833(3)
Cell volume V (Å ³)	244.735(2)	230.612(2)	229.199(4)
Perovskite parameter (a _p =V ^{1/3} /2) (Å)	3.1275	3.0662	3.0600
Spontaneous strain (s)	0.033	0.022	0.012
Crystallite size (nm)	102.96(3)	128.53(6)	120.32(3)
Microstrain	0.0014(4)	0.00038(1)	0.0009(1)
Atomic Occupancies			
Nd	0.985(1)	0.855(4)	0.854(1)
Na/ K	0	0.144(5)	0.145(1)
Mn	1	1	1
O	1.01(4)	1.00(1)	1.013(4)
Fractional Co-ordinates			
Nd/K/Na: (x, y, 0.25)			

x	-0.0054(1)	-0.0052(2)	-0.0003(0)
y	0.0501(4)	0.0462(1)	0.0372(2)
Mn: (0, 0, 0.5)			
O1: (x, y, 0.25)			
x	0.0820(2)	0.0744(3)	0.0703(2)
y	0.5027(2)	0.4788(0)	0.4649(1)
O2: (x, y, z)			
x	0.7074(3)	0.7109(4)	0.7252(2)
y	0.3008(0)	0.2848(0)	0.2796(5)
z	0.0449(1)	0.0484(4)	0.0499(2)

Structural and microstructural parameters calculated from Rietveld refinement (Figure 2) of XRD patterns of three compounds are listed in Table-2. Lattice parameters are little deviated from actual ICSD values for all three compounds. Lattice parameters of three compounds can be expressed as $\mathbf{a} \approx \mathbf{b} \approx \frac{c}{\sqrt{2}}$. The undoped and Na-doped NdMnO₃ compounds take O' type orthorhombic structure in which $\frac{c}{\sqrt{2}} < \mathbf{a} < \mathbf{b}$ and K-doped NdMnO₃ compound takes O type orthorhombic structure with $\mathbf{a} < \frac{c}{\sqrt{2}} < \mathbf{b}$.¹² The O' type structure originates from strong Jahn-Teller effect which distorts the MnO₆ octahedra. The O type structure is more symmetrical than O' in which distortion is less. Though the ionic radii of Na⁺(1.39Å) or K⁺(1.64Å) is greater than Nd⁺³(1.27Å) in a 12 coordination system,³⁵ the unit cell volumes of doped compounds are less than that of the undoped compound. Alonso et al¹² reported the unit cell volume of NdMnO₃ as 238.65Å³ from neutron diffraction measurements. Samantaray et al²⁷ reported the unit cell

volume of $\text{Nd}_{0.85}\text{K}_{0.15}\text{MnO}_3$ as 231.6 \AA^3 and Lakshmi and Reddy²⁶ reported that of $\text{Nd}_{0.85}\text{Na}_{0.15}\text{MnO}_3$ as 226.76 \AA^3 . Thus, our results are comparable and very close to the reported values. The possible reason for the decrease in unit cell volume is due to monovalent doping by substitution of equivalent amount of Nd^{3+} , which in turn results in shortening of Mn-O bond lengths and thereby decrease in the volume of the MnO_6 octahedra. In the present case, 15mol% monovalent doping results into 30% conversion of Mn^{+3} ions into Mn^{+4} ions to maintain the charge neutrality in the compound. This is a common occurrence in rare earth doped manganates.⁶ The decrease in Mn-O bond length is primarily due to the replacement of Mn^{+3} ions (0.58 \AA) by smaller Mn^{+4} ions (0.53 \AA) in a 6 co-ordination system.³⁵ It is interesting to note that mixed valency of Mn was not detected in undoped NdMnO_3 as Nd exhibits a strong basic character, suitable to stabilize Mn^{+4} .¹² Replacement of 30% Mn^{+3} by Mn^{+4} ions reduces the lattice distortion as Mn^{+3} ions are primarily responsible for Jahn-Teller effect. Introduction of non Jahn-Teller Mn^{+4} ions increases the structural symmetry of the system. Due to doping, the difference between two lattice parameters ($|\mathbf{a} - \mathbf{b}|$) decreases [Table 2] and the crystal structure moves towards a tetragonal unit cell, thereby advancing towards a more structural symmetry. The perovskite parameter a_p reduces due to doping as the radius of Mn^{+4} is smaller than Mn^{+3} . The spontaneous orthorhombic strain¹² is defined as $s = \frac{2(b-a)}{a+b}$ and shown in Table 2. It is a measure of tilting/ distortion of the octahedra and a decrease in 's' means decrease in lattice distortion. It is found that 's' continuously decreases with an increase in dopant radius. The crystallite size and r.m.s. microstrain values obtained from Rietveld refinement analysis are reported in Table 2. An increase in crystallite size and decrease in r.m.s. microstrain is noticed for all three compounds in comparison to powders sintered at 800°C (Table 1). It suggests that sintering at higher temperature results, in general, more structural stability in the compounds. It

is also to be noted that the spontaneous strain and r.m.s. strain in all three compounds follow the same nature of variation. The refined atomic occupancies and atomic co-ordinates of each atom present in the compounds are also tabulated in Table 2. From the calculated occupancies of Nd, Na, K and O, the actual chemical compositions are found out to be $\text{Nd}_{0.985}\text{MnO}_{3.03}$, $\text{Nd}_{0.855}\text{Na}_{0.144}\text{MnO}_3$ and $\text{Nd}_{0.854}\text{K}_{0.145}\text{MnO}_{3.04}$.

Microstructure characterization by HRTEM

Structural confirmations and microstructure characterizations of undoped and 15mol% Na- and K-doped NdMnO_3 compounds sintered at 1000°C for 10h are carried out by HRTEM analysis. The HRTEM images of undoped NdMnO_3 compound are presented in Figure 3. It has been observed that the compound is composed of tiny single crystals. The particle size of one isolated spherical single particle is found to be 109.4nm [Figure 3(a)] which is close to crystallite size obtained from Rietveld refinement (103nm). The core-shell structure of this particle is noticed and shown in Figure 3(b) with a crystalline core and an amorphous like shell with a radius of 8.84nm. The crystalline core is made up by parallel set of lattice fringes corresponding to most intense (112) planes with interplanar distance $d \sim 2.7\text{\AA}$ [Figure 3(c)]. Another well grown orthorhombic shaped single crystal along the easy axis with $\sim 550\text{nm}$ size has been identified [Figure 3(d)]. The phase formation of the NdMnO_3 compound is verified by the indexed selected area electron diffraction (SAED) pattern (Figure 3(e)). It is evident that all diffraction spots are aligned in different layer lines. The distance between two consecutive spots in a layer line is proportional to c^* axis of the orthorhombic unit cell and all other spots are indexed accordingly. These spots are identical with the powder diffraction pattern of the undoped compound as shown in Figure 2 and the phase confirmation has also been established by electron diffraction pattern. Absence of powder ring pattern confirms the formation of tiny single crystal of the compound

after sintering at 1000°C. The EDAX spectra are shown in Figure 3(f) and the compositional analysis is tabulated in Table-3. The composition is very close to the calculated composition from Rietveld refinement.

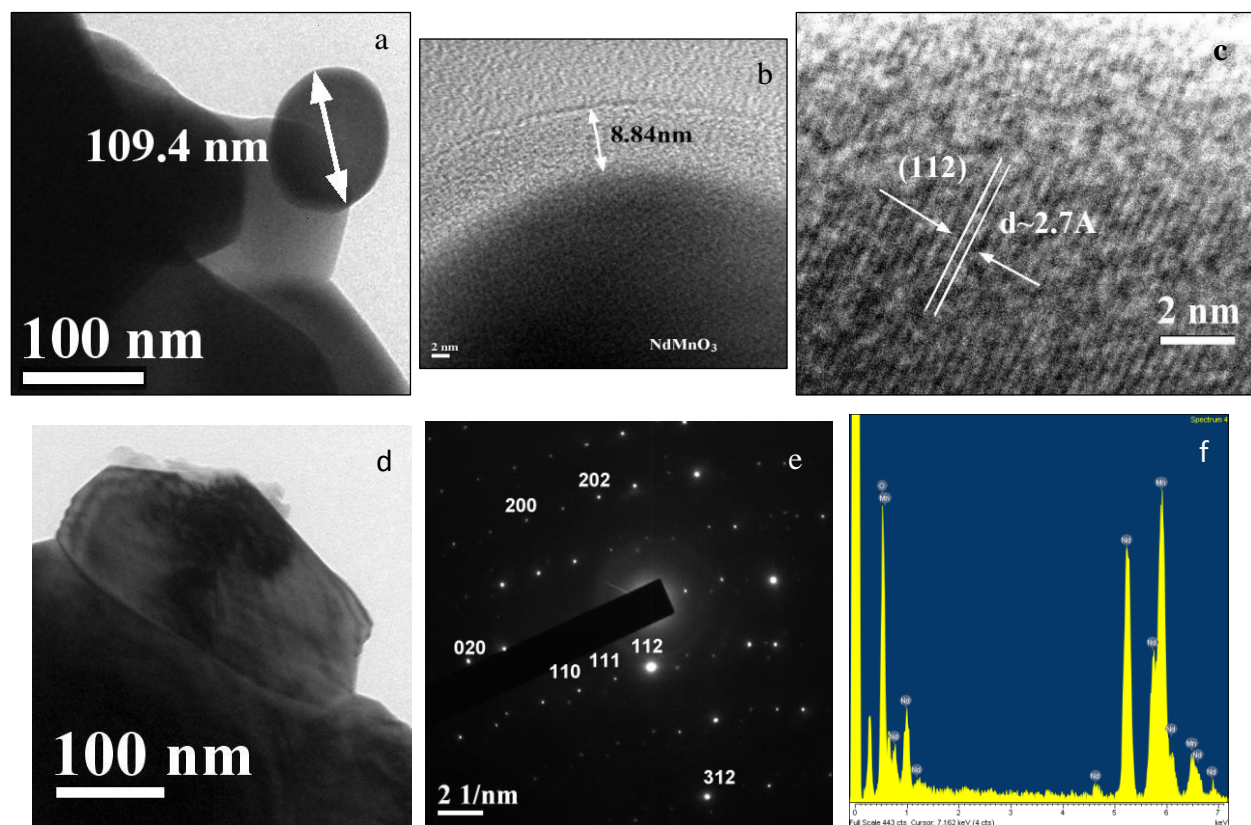


Fig. 3 HRTEM images of 1273K sintered NdMnO₃(a) isolated spherical single crystal, (b) core-shell structure of the single crystal, (c) lattice fringe pattern of the core, (d) isolated orthorhombic shaped single crystal and (e) electron diffraction pattern of orthorhombic single crystal (f) EDAX spectra.

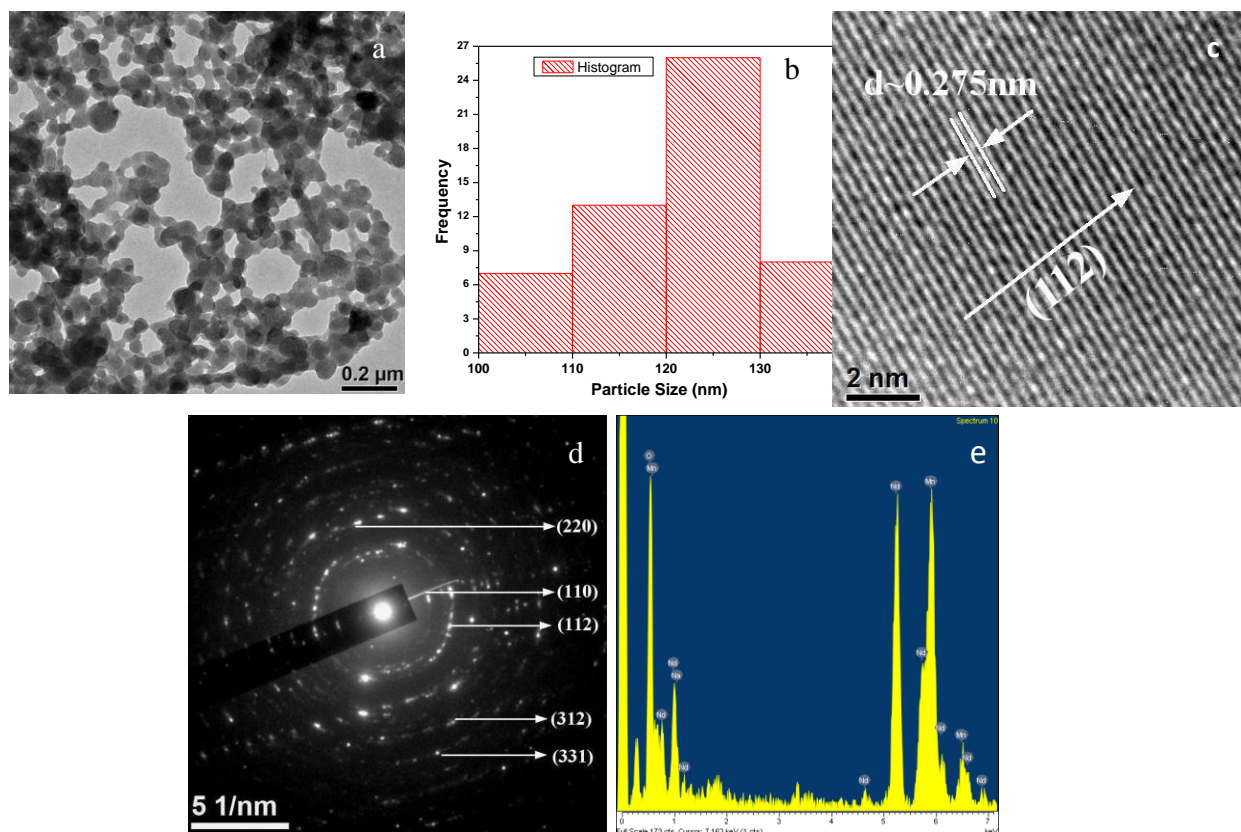


Fig. 4 HRTEM images of $\text{Nd}_{0.85}\text{Na}_{0.15}\text{MnO}_3$ sintered at 1273K: (a) spherical tiny single crystals (particles), (b) size distribution histogram of spherical particles, (c) lattice fringe pattern and (d) SAED pattern (e) EDAX spectra.

Some HRTEM images of $\text{Nd}_{0.85}\text{Na}_{0.15}\text{MnO}_3$ compound sintered at 1000°C are shown in Figure 4. It is evident that the compound is composed of spherical tiny single crystals (particles) of almost uniform dimension and shape [Figure 4(a)]. Size distribution histogram of these spherical particles is shown in Figure 4(b) where the range of particle size varies between 100 to 140nm and most of the particles are in the range 120 to 130nm – similar to the crystallite size of 128nm obtained from Rietveld analysis. Lattice fringe pattern obtained from an isolated particle is shown in Figure 4(c) and the most intense (112) reflection has been identified with interplanar spacing 0.275 nm. The SAED pattern in Figure 4(d) reveals the presence of layer

line structure overlapped with powder diffraction ring patterns, resulting from the random orientations of the tiny single crystals. Some of the intense rings are identified and properly indexed with the corresponding crystal planes. The EDAX spectrum is shown in Figure 4(e) and the compositional analysis is tabulated in Table-3. The composition is very close to the expected composition.

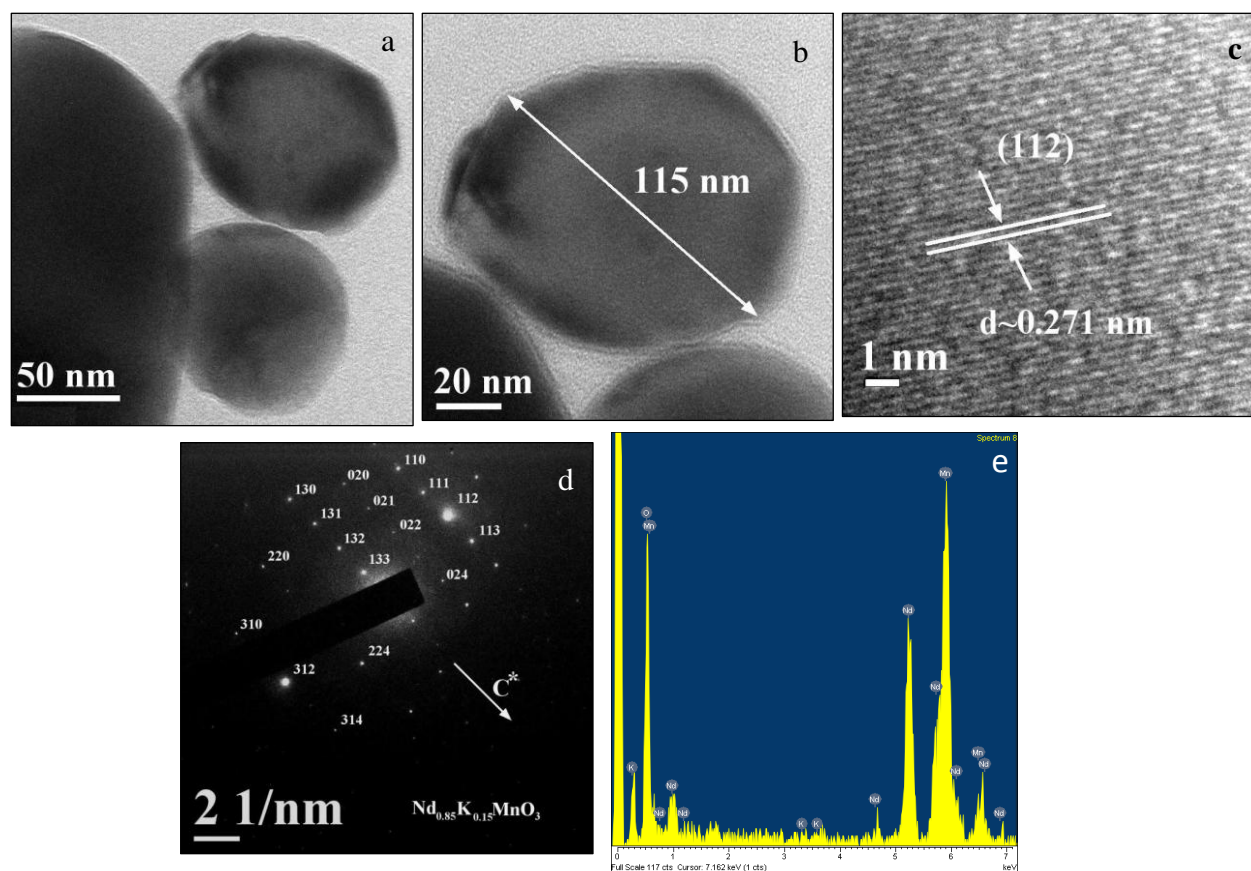


Fig. 5 HRTEM images of $\text{Nd}_{0.85}\text{K}_{0.15}\text{MnO}_3$ compound sintered at 1273K: (a) some isolated spherical single crystals (particles) (b) an isolated single crystal (c) lattice fringe pattern (d) SAED pattern (e) EDAX spectra.

HRTEM images of the $\text{Nd}_{0.85}\text{K}_{0.15}\text{MnO}_3$ compound sintered at 1000°C are shown in Figure 5. Image of some spherical single crystals (particles) is shown in Figure 5(a) and enlarged

image of an isolated spherical particle is shown in Figure 5(b). The measured particle size of 115 nm is close to the crystallite size 120 nm obtained from Rietveld refinement of this compound. The most intense (112) reflecting plane with interplanar spacing 0.271 nm has been identified from the lattice fringes and shown in Figure 5(c). Instead of powder ring pattern, single crystal diffraction pattern with distinct layer lines from an isolated crystal is recorded and shown in Figure 5(d). From these spots the c^* axis has been identified and most of the intense reflections are indexed accordingly. These indexed reflections are also present in the corresponding XRD pattern of the compound with respective relative intensities. The EDAX spectrum is shown in Figure 5(e) and the compositional analysis is tabulated in Table-3.

Table 3: Compositional analysis from EDAX

Sample	Element	Weight%	Atomic%
NdMnO ₃	O K	16.08	54.34
	Mn K	23.29	22.93
	Nd L	60.63	22.73
Nd _{0.85} Na _{0.15} MnO ₃	O K	16.48	54.58
	Na K	0.81	1.87
	Mn K	22.02	21.25
	Nd L	60.69	22.30

Sample	Element	Weight%	Atomic%
Nd _{0.85} K _{0.15} MnO ₃	O K	17.94	55.59
	K K	0.77	0.98
	Mn K	27.75	25.02
	Nd L	53.53	18.39

3D representation of the structure and measurement of Bond length-Bond angle

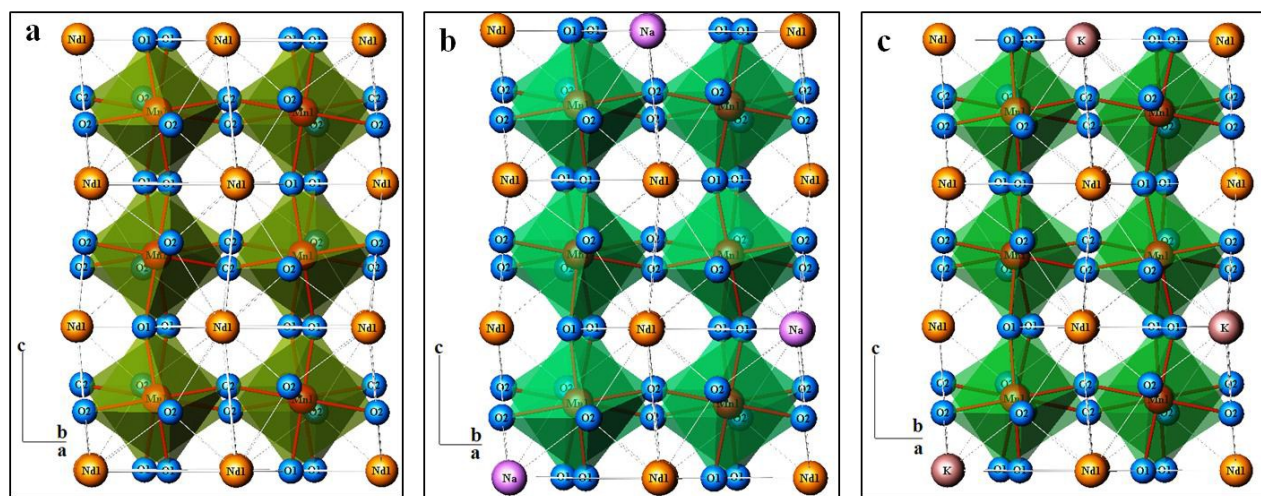


Fig. 6 Crystal structures of (a) NdMnO₃, (b) Nd_{0.85}Na_{0.15}MnO₃ and (c) Nd_{0.85}K_{0.15}MnO₃ compounds.

Crystal structures of undoped and 15mol% Na- and K-doped single phase NdMnO₃ compounds are generated using refined lattice parameters and atomic co-ordinates. Both undoped and doped compounds are crystallized in perovskite structure with orthorhombic unit cell and the respective 3D structure models are shown Figure 6. In these compounds Nd⁺³, Mn⁺³

cations and O^{2-} anions occupy corner, body centre and face centre positions respectively. MnO_6 octahedra are formed with Mn atom at octahedral position and 6 oxygen atoms at the octahedral corners. Crystal structure of undoped $NdMnO_3$ is shown in Figure 6(a). Mn atoms (red balls) occupy the centre of the MnO_6 octahedron (green color) and these octahedra are tilted to each other. Figures 6(b) and 6(c) represent the structures of $Nd_{0.85}Na_{0.15}MnO_3$ and $Nd_{0.85}K_{0.15}MnO_3$ compounds respectively. All the compounds are grown along their easy axis **c**. In these compounds, 15mol% of Nd^{+3} ions are replaced by Na^+ or K^+ ions as shown in these Figures. In rare earth manganate perovskite structures Mn-O-Mn bond angle and Mn-O bond lengths along with R-O bond lengths play significant role in determining the behavior and properties of these compounds.¹⁻⁴ Doping by monovalent atom at Nd position modifies these parameters and thereby tunes their magnetic and electrical properties. A small change in Mn-O-Mn bond angle and bond length changes the degree of tilting of the octahedra and Jahn-Teller distortion. Lattice distortion and thus degree of tilting of the MnO_6 octahedra can be measured theoretically by Goldsmith tolerance factor and experimentally by measuring Mn-O bond lengths and Mn-O-Mn bond angle. The Goldschmidt tolerance factor is defined as:¹¹

$$t = \frac{\langle r_A \rangle + r_O}{\sqrt{2}(\langle r_B \rangle + r_O)} = \frac{d_{A-O}}{\sqrt{2}(d_{Mn-O})}$$

where r_A is the average ionic radius at A-site of ABO_3 type compound, r_B and r_O are the ionic radii of B-site and oxygen respectively, d_{A-O} is the average A-O bond length. For a perfectly undistorted cubic perovskite structure with a tolerance factor value of 1.0, six Mn-O bonds of MnO_6 octahedron are of equal lengths and Mn-O-Mn bond angles are 180° . But for a distorted perovskite structure, octahedra are tilted with different Mn-O bond lengths in different directions and Mn-O-Mn bond angle is less than 180° with a tolerance factor value less than 1.0. As in the present case, 15 mol% of Nd^{+3} has been replaced by equivalent amount of monovalent K^+ or

Na^+ , the ionic radius of A site has been taken as the weighted average of Nd^{+3} and K^+/Na^+ ionic radii. It is customary to consider A site cation in 12 co-ordination, Mn in six co-ordination and O in two co-ordination system for orthorhombic rare earth perovskite manganates.¹² The ionic radii of Na^+ (1.39Å) or K^+ (1.64Å) is greater than Nd^{+3} (1.27Å) in a 12 co-ordination system.³⁵ Thus, doping by K^+ increases the tolerance factor and thereby ensures a better structural stability of the K-doped compound. A 15mol% Na- and K- doping in NdMnO_3 changes (i) Mn-O-Mn bond angles, (ii) Nd-O bond lengths and (iii) Mn-O bond lengths in different directions. The order of ionic radii is Nd^{+3} (1.27Å) < Na^+ (1.39Å) < K^+ (1.64Å)³⁵ and the similar order is also followed for bond angles and bond lengths and thereby the degree of distortions. R-O and Mn-O bond lengths and Mn-O-Mn bond angles for the undoped and 15mol% Na- and K-doped NdMnO_3 compounds are measured and given in Table 4. Mn-O bond lengths of undoped and doped NdMnO_3 are graphically represented in Figure 7. The average Mn-O bond length is close to the sum of ionic radii ($r_{\text{Mn}^{+3}} + r_{\text{O}} = 1.93\text{Å}$). In these compounds there are one pair of Mn-O1 and two pairs of Mn-O2 bonds of different bond lengths. Different Mn-O bond lengths in different directions reveal a stronger Jahn-Teller distortion in octahedral.¹³ The maximum and minimum stretching of Mn-O bonds are 2.09 and 2.00Å respectively in the undoped compound [Figure 7(a)] and stretching in doped compounds are, in general, somewhat less than that the undoped compound [Figures 7(b) & (c)]. The average bond length, $\langle \text{Mn-O} \rangle_a$ decreases from 2.03 (undoped) to 1.99 for Na-doped and to 1.98 for K-doped compound. Therefore, doping by larger ions reduces the stretching of Mn-O bond in MnO_6 octahedra. This helps reducing J-T distortion in the doped compounds. There are two pairs of Nd-O1 and three pairs of Nd-O2 bonds in these compounds. It is evident that all these bond lengths are reduced in comparison to those of undoped compound and the average $\langle \text{Nd-O} \rangle_a$ bond length in undoped compound also reduces in doped compounds. It

suggests that doped compounds have better ionic packing than the undoped compound as well as unit cell volumes of doped compounds are also less, as has been reported in Table 2. Increase in tolerance factor (t) with doping indicates a better symmetry for the doped compounds.

Table 4: Bond lengths, bond angles, MnO_6 octahedra tilting and distortion parameters revealed from Rietveld structure refinements of undoped and doped NdMnO_3 compounds.

Compounds	NdMnO_3	$\text{Nd}_{0.85}\text{Na}_{0.15}\text{MnO}_3$	$\text{Nd}_{0.85}\text{K}_{0.15}\text{MnO}_3$
Bond lengths (Å)			
Mn-O1(×2)	2.00(1)	1.97(1)	1.97(0)
Mn-O2(×2)	2.01(1)	1.96(7)	1.96(1)
Mn-O2(×2)	2.09(2)	2.04(2)	2.00(0)
<Mn-O>_a	2.03	1.99	1.98
Nd-O1	2.35(2)	2.36(7)	2.36(8)
Nd-O1	2.62(7)	2.43(8)	2.38(1)
Nd-O2(×2)	2.41(0)	2.39(5)	2.42(0)
Nd-O2(×2)	2.66(4)	2.55(2)	2.52(2)
Nd-O2(×2)	2.71(2)	2.74(5)	2.79(7)
<Nd-O>_a	2.57	2.52	2.53
$t = d_{\text{Nd-O}}/\sqrt{2} d_{\text{Mn-O}}$	0.89	0.895	0.903
Bond angles between two adjacent MnO_6 octahedra (deg.)			
Mn-O1-Mn(×2)	153.7(7)	155.2(5)	154.9(0)
Mn-O2-Mn (×4)	151.2(2)	152.8(3)	154.4(8)
<cos²θ>	0.78	0.80	0.82

$\langle \omega \rangle$	27.93	26.4	25.37
--------------------------	-------	------	-------

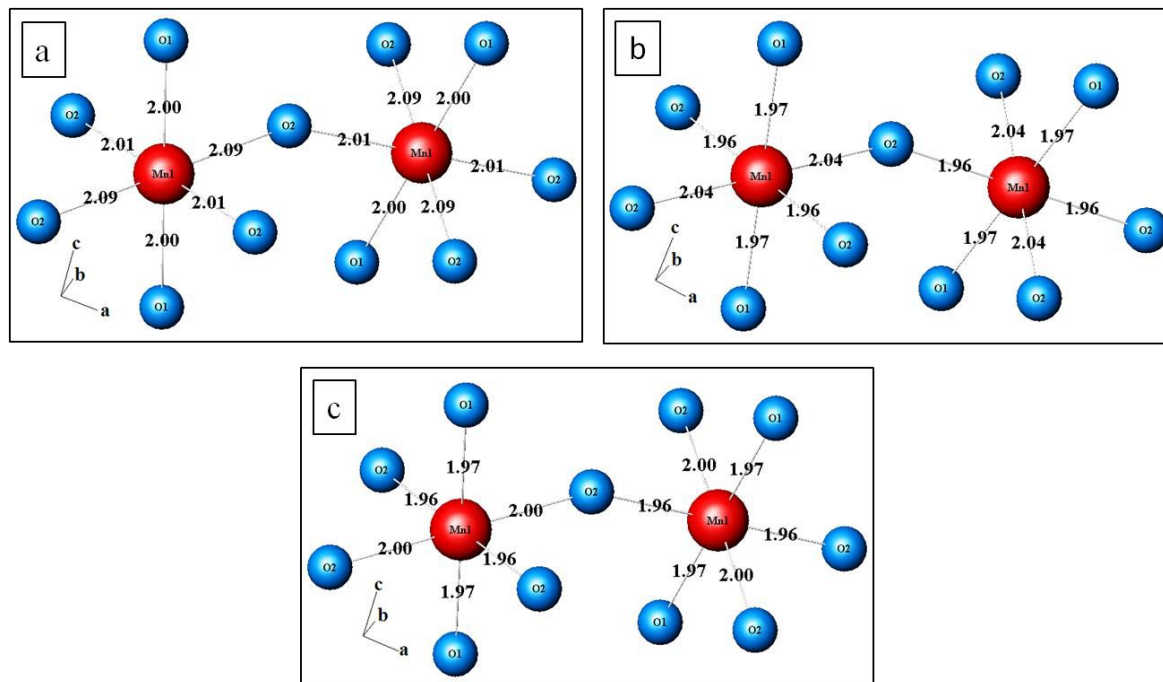


Fig. 7 Mn-O bond lengths in (a) NdMnO_3 , (b) $\text{Nd}_{0.85}\text{Na}_{0.15}\text{MnO}_3$, and (c) $\text{Nd}_{0.85}\text{K}_{0.15}\text{MnO}_3$ compounds.

Another important parameter describing octahedral tilting angle (θ) between two adjacent octahedra which are manifested by angle between different Mn-O-Mn bonds in these octahedra. All Mn-O-Mn bond angles between two adjacent octahedra are listed in Table-4 and shown in Figures 8, 9 and 10 for NdMnO_3 , $\text{Nd}_{0.85}\text{Na}_{0.15}\text{MnO}_3$, and $\text{Nd}_{0.85}\text{K}_{0.15}\text{MnO}_3$ compounds respectively. Both Mn-O1-Mn and Mn-O2-Mn bond angles are significantly lower than 180° in all three compounds and the tilting angle θ in doped compounds are somewhat higher than the undoped compound. Two types of octahedral tilting in undoped compound are shown in Figure 8. In Figure 8(a), tilting between two adjacent octahedra is shown with different tilting angles in

two different directions. It may also be noted that the O1-Mn-O1 and O2-Mn-O2 bond angles are 180° . However, the individual O-Mn and Mn-O bond angles are not identical with 90° which is shown in Figure 8(b). It indicates that the individual octahedron also contains distortions arising both from asymmetry in Mn-O bond lengths and bond angles. The tolerance factor t is directly proportional to $\cos^2\theta$ and thus $\cos^2\theta$ value effectively measures the degree of distortion.⁶ The average $\langle \cos^2\theta \rangle$ value increases with doping thereby introducing more symmetry in the structure. The ω measures the deviation of average Mn-O-Mn bond angle from the ideal value of 180° . The average $\langle \omega \rangle$ values in doped compounds are less than the undoped compound. It further suggests that doped compounds are more symmetrical than the undoped compound.

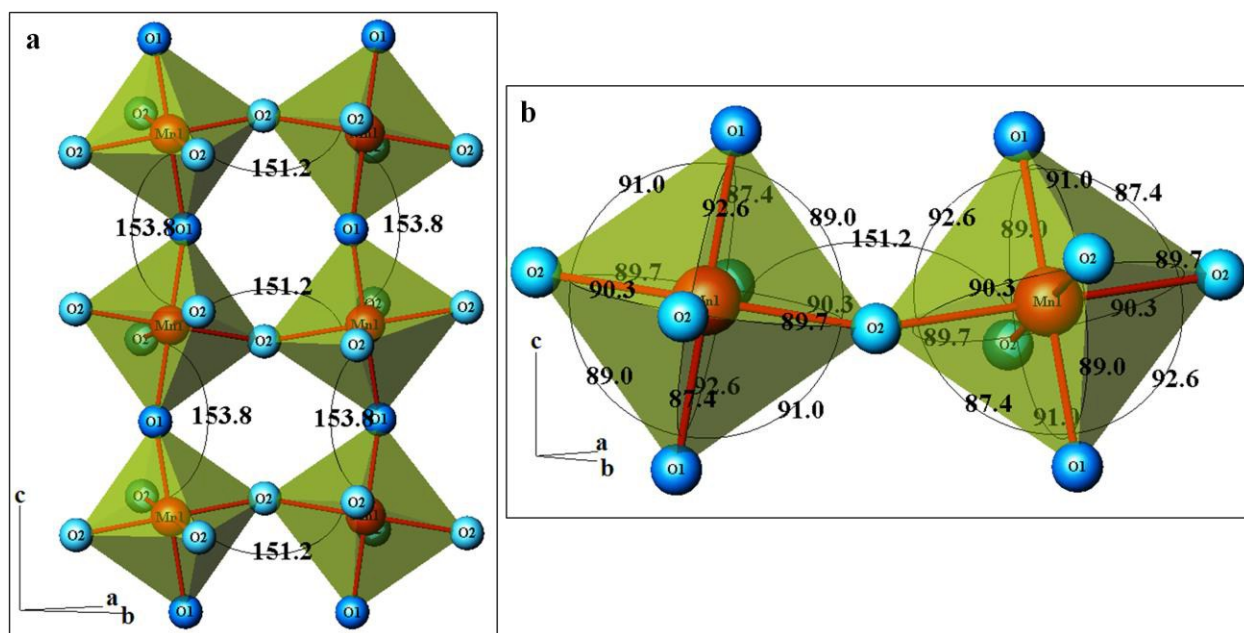


Fig. 8 (a) Mn-O1-Mn and Mn-O2-Mn bond angles between two adjacent octahedra of NdMnO₃ and (b) asymmetrical Mn-O bond angles in individual MnO₆ octahedron.

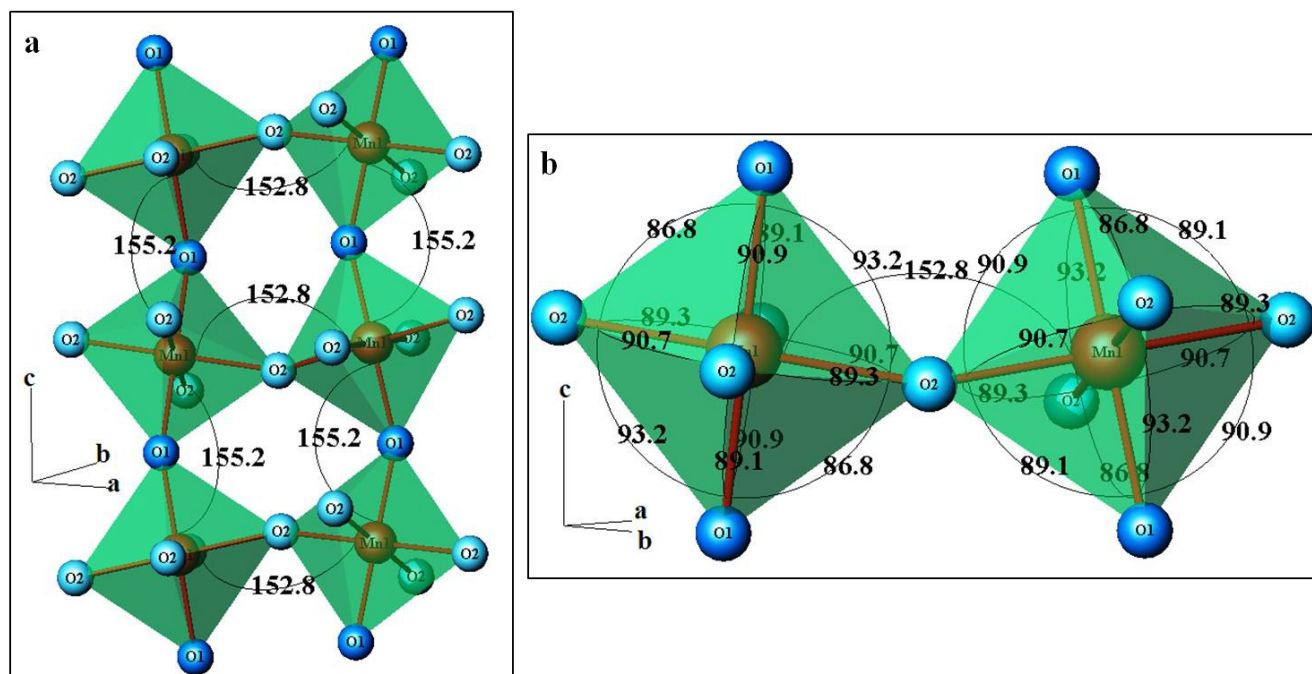


Fig. 9 (a) Mn-O1-Mn and Mn-O2-Mn bond angles between two adjacent octahedra and (b) asymmetrical Mn-O bond angles in individual octahedron of $\text{Nd}_{0.85}\text{Na}_{0.15}\text{MnO}_3$ compound.

Tilting angles are somewhat higher in Na-doped compound [Figure 9(a)] and the distortion in individual octahedron is also less compared to undoped compound [Figure 9(b)]. It indicates that the Na-doped compound has better symmetry as well as better structural stability than the undoped compound.

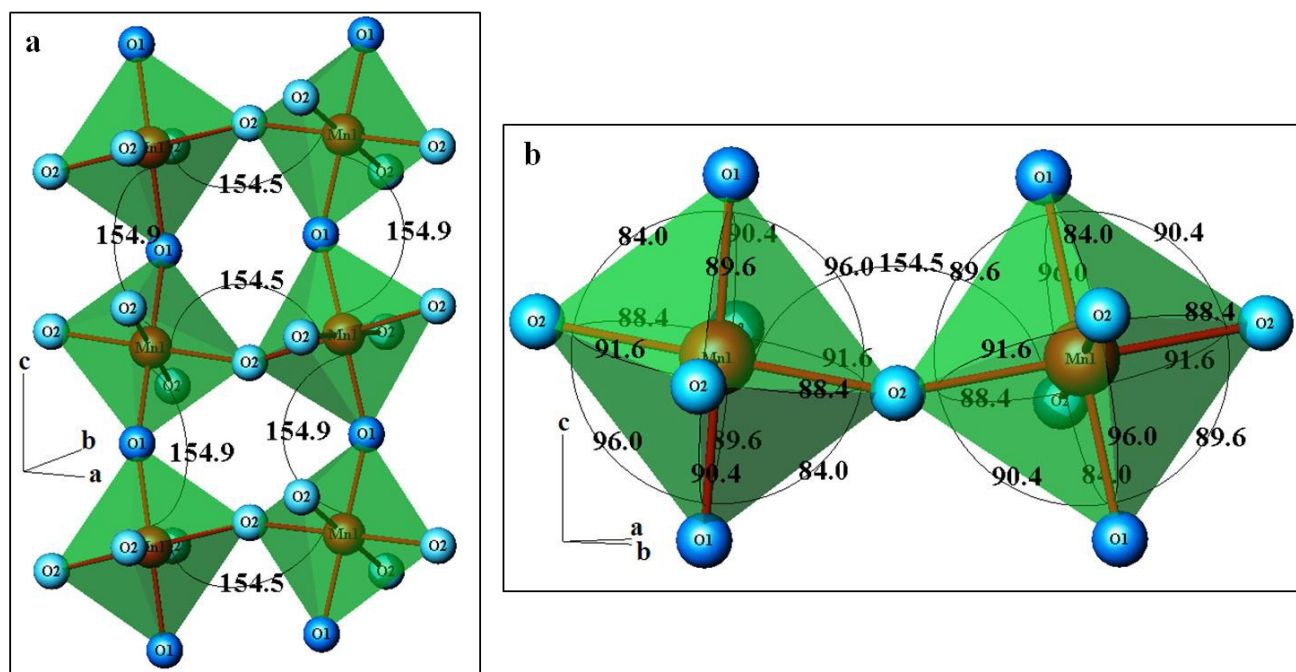


Fig. 10 (a) Mn-O1-Mn and Mn-O2-Mn bond angles between two adjacent octahedra and (b) asymmetrical Mn-O bond angles in individual octahedron of $\text{Nd}_{0.85}\text{K}_{0.15}\text{MnO}_3$ compound.

In the case of K-doped compound tilting angles are higher than Na-doped compound [Figure 10(a)] and the distortion in individual octahedron is also less in comparison to both undoped and Na-doped compound [Figure 10(b)]. It thus indicates that the K-doped compound has better symmetry as well as better structural stability than both the undoped and Na-doped compounds. These changes in Mn-O bond lengths and Mn-O-Mn bond angles due to doping should be advantageous in magnetic behavior of the compound which is discussed in the next section.

DC Magnetization

Temperature dependent dc magnetization behavior is studied for all NdMnO_3 , $\text{Nd}_{0.85}\text{Na}_{0.15}\text{MnO}_3$ and $\text{Nd}_{0.85}\text{K}_{0.15}\text{MnO}_3$ compounds in the temperature range of 30K to 300K.

Zero field cooled (ZFC) and Field cooled (FC) curves under 500 Oe constant magnetic field is shown in Figure 11. Undoped NdMnO_3 is known to have a paramagnetic to anti-ferromagnetic phase transition with lowering of temperature.¹³ This anti-ferromagnetic type behavior comes from Mn^{+3} - Mn^{+3} super exchange mechanisms. In this study, the M-T behavior of NdMnO_3 shown in Figure 11(a) affirms the anti-ferromagnetic behavior. A large divergence between ZFC and FC magnetization is observed under 50K which signifies the presence of anti ferromagnetic coupling in the compound.³⁶ Derivative of field cooled M-T plot is shown in the inset of Figure 11(a). The paramagnetic to anti-ferromagnetic transition temperature (Neel temperature, T_N) is found to be 67.2K from this plot. The ZFC and FC magnetization curves of $\text{Nd}_{0.85}\text{Na}_{0.15}\text{MnO}_3$ are shown in Figure 11(b). 15mol% monovalent doping transforms 30% Mn^{+3} to Mn^{+4} , and Zener double exchange mechanism³⁷ in Mn^{+3} - O^{2-} - Mn^{+4} network comes into play. This strong ferromagnetic interaction rules over the weak anti-ferromagnetic superexchange interactions in Mn^{+3} - Mn^{+3} , Mn^{+4} - Mn^{+4} and Mn^{+4} - O^{2-} - Mn^{+4} networks. This results the 15mol% Na doped compound to exhibit a paramagnetic to ferromagnetic transition with lowering of temperature. The paramagnetic-ferromagnetic transition temperature or Curie temperature (T_C) is found to be 99.1K from the derivative of M-T plot (shown in inset of Figure 11b). Very similar behavior is also noticed in $\text{Nd}_{0.85}\text{K}_{0.15}\text{MnO}_3$ compound. The ZFC and FC curves for $\text{Nd}_{0.85}\text{K}_{0.15}\text{MnO}_3$ compound are shown in Figure 11(c) and the T_C is found to be 98.6K. Thus, monovalent doping has a large advantage of transforming anti-ferromagnetic NdMnO_3 compound to a ferromagnetic one at low temperature. Doping also extends the transition temperature from 67K to 99K which allows the compound to be in ferromagnetic state in a higher temperature range. The paramagnetic region of temperature dependent reciprocal susceptibility follows the Curie law for all three compounds. T_C values of 15% Na and K doped compounds are almost same. This

suggests that for similar doping level with different monovalent dopants, T_C values are nearly equal if the tolerance factor is less than 0.905. An insignificant increase in T_C with tolerance factor upto a T_C value 0.905 can also be noticed from the universal curve of T_C vs tolerance factor for 30% divalent cation doped RMnO_3 system.⁶ 15% monovalent doping and 30% divalent doping- both converts 30% Mn^{3+} to Mn^{4+} which is the reason for similar kind of T_C variation with tolerance factor.

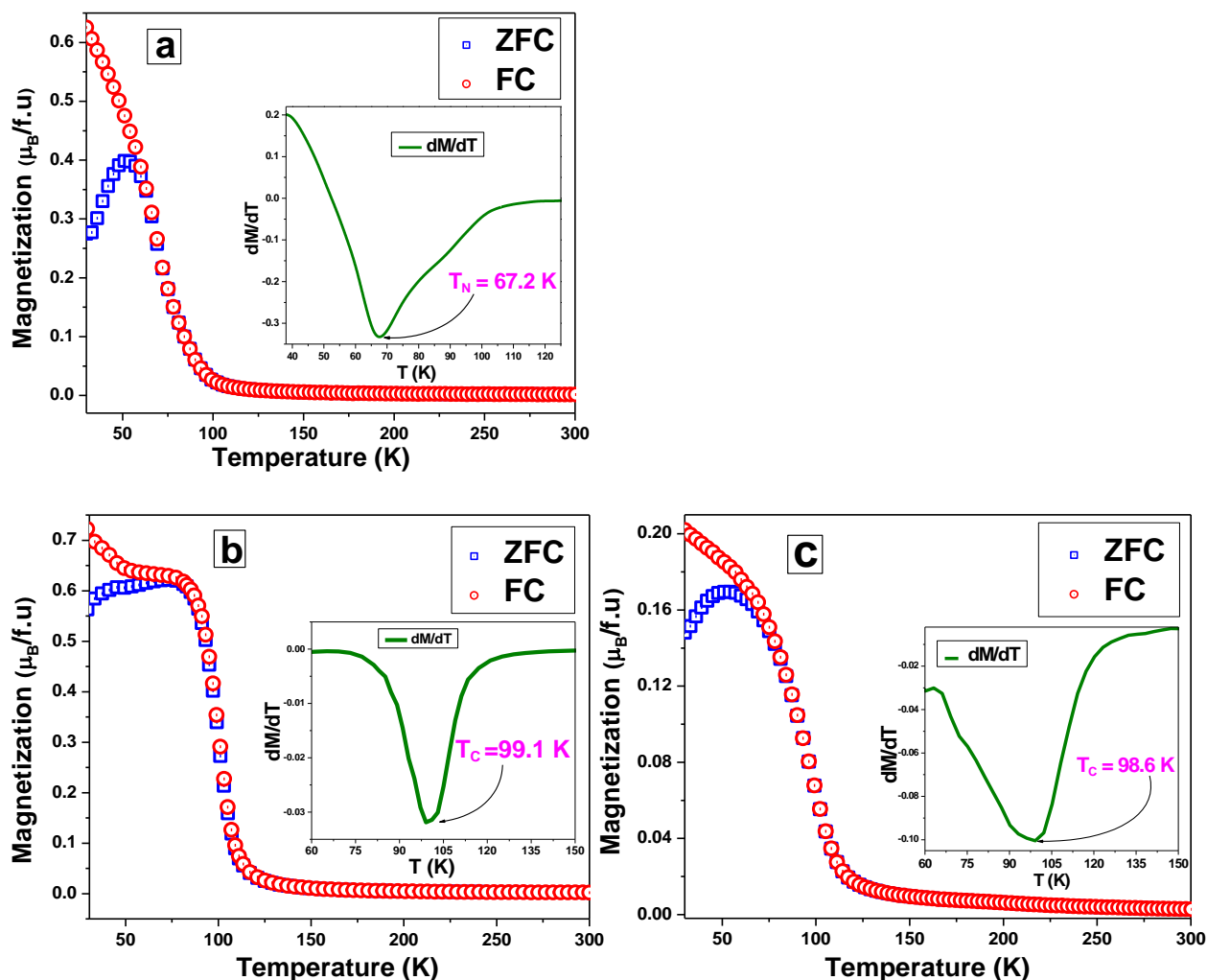


Fig. 11 Temperature dependent magnetization curves for (a) NdMnO_3 , (b) $\text{Nd}_{0.85}\text{Na}_{0.15}\text{MnO}_3$, and (c) $\text{Nd}_{0.85}\text{K}_{0.15}\text{MnO}_3$ compounds. Inset shows the derivative of M (FC) against temperature.

Conclusion

ABO₃ type perovskite structured rare earth manganate NdMnO₃ and its monovalent doped derivatives Nd_{0.85}K_{0.15}MnO₃ and Nd_{0.85}Na_{0.15}MnO₃ are studied critically to analyze the effect of different monovalent cation doping with same doping level on structure, lattice and octahedral distortion of NdMnO₃ in details. The compounds are prepared in single crystalline form by conventional sol-gel method in a very short duration. All compounds are sintered at 800°C and 1000°C to study the effect of sintering temperature on the formation of the compound. Structures of all three compounds belong to orthorhombic with P_{bnm} space group. Undoped and Na doped compound takes an O' type orthorhombic structure but K-doped compound takes a more symmetrical O type structure. Microstructural parameters like crystallite size and r.m.s. lattice strain and structural parameters like lattice parameters, space groups and atomic fractional coordinates of all three compounds are revealed from the Rietveld refinements of respective XRD patterns. Microstructures are also revealed from HRTEM image analysis and a defect free single phase growth of the compounds in tiny single crystal form is established. The unit cell and octahedral arrangements clearly established that both 15mol% monovalent doping of Na-and K- results in better symmetry and structure stability in the doped compounds. Measurements of Mn-O, Nd-O bond lengths and Mn-O-Mn bond angle and thereby tolerance factor calculations show that monovalent doping induces a better structural symmetry in NdMnO₃. An increase in dopant ionic radius proves to achieve better structural symmetry. Undoped NdMnO₃ compound is found to have a paramagnetic to anti-ferromagnetic transition with T_N as 67.2K where as 15mol% Na- and K-doped compounds show a paramagnetic to ferromagnetic transition with T_C ≈ 99K. Thus, monovalent doping is also proved to be successful in tuning the magnetic property of the

compound. Same doping level (15%) with two different monovalent dopants (Na and K) causes nearly same T_c in doped NdMnO_3 compounds.

Acknowledgements

Authors wish to thank the UGC-DAE consortium for Scientific Research, Kolkata Centre for providing the SQUID facility. DST is acknowledged for providing fund toward an X-ray diffractometer. SKP wishes to thank UGC for the financial assistance through the 'Centre of Advanced Study under the thrust area Condensed Matter Physics including laser applications'.

References

- (1) C.N.R. Rao and B. Raveau, *Colossal Magnetoresistance, Charge Ordering and Related Properties of Manganese Oxides*, World Scientific, Singapore, 1998.
- (2) Y. Tokura, *Colossal Magneto-Resistive Oxides*, Gordon and Breach, London, 2000.
- (3) Y. Tokura and Y. Tomioka, *J. Magn. Magn.Mater.* 1999, **200**, 1-23.
- (4) C. N. R. Rao, A. Arulraj, P.N. Santosh and A.K. Cheetham, *Chem. Mater.*, 1998, **10**, 2714-2722.
- (5) C. N. R. Rao, A. Arulraj, A.K. Cheetham and B. Raveau, *J. Phys.: Condens. Matter*, 2000, **12**, R83–R106.
- (6) P. K. Siwach, H. K. Singh and O. N. Srivastava, *J. Phys.: Condens. Matter*, 2008, **20**, 273201-43.
- (7) H. Taguchi, M. Io, M. Yoshinaka, K. Hirota and O. Yamaguchi, *Solid State Ionics*, 2004, **172**, 611 –615.

- (8) S. Jandl, V. Nekvasil, M. Divis, A.A. Mukhin, J. Holsa and M.L. Sadowski, *Phys. Rev. B*, 2005, **71**, 024417 1-6.
- (9) P. G. Radaelli, M. Marezio, H.Y. Hwang, S.W. Cheong and B. Batlogg, *Phys. Rev. B*, 1996, **54**, 8992-8995.
- (10) P. G. Radaelli, G. Iannone, M. Marezio, H.Y. Hwang, S.W. Cheong, J.D. Jorgensen and D.N. Argyriou, *Phys. Rev. B*, 1997, **56**, 8265- 8276.
- (11) V. M. Goldschmidt, *Goechemistry*, Oxford, Oxford University Press, 1958.
- (12) J. A. Alonso, M. J. Martinez-Lope, M. T. Casais and M. T. Fernandez-Diaz, *Inorg. Chem.*, 2000, **39**, 917-923.
- (13) A. Munoz, J. A. Alonso, M. J. Martinez-Lope, J. L. Garcia-Munoz and M. T. Fernandez-Diaz, *J. Phys.: Condens. Matter*, 2000, **12**, 1361–1376.
- (14) W. H. Li, S.Y. Wu, K.C. Lee and J.W. Lynn, *Physica B*, 2000, **276-278**,724-725.
- (15) S. Y. Wu, C. M. Kuo, H. Y. Wang, W. H. Li, K. C. Lee, J. W. Lynn and R. S. Liu, *J. Appl. Phy.*, 2000, **87**, 5822-5824.
- (16) B. Dabrowski, S. Kolesnik, A. Baszczuk, O. Chmaissem, T. Maxwell and J. Mais, *J. Solid State Chem.*, 2005, **178**, 629–637.
- (17) T. Chatterji, B. Ouladdiaf and D. Bhattacharya, *J. Phys.: Condens. Matter*, 2009, **21**, 306001(5pp).
- (18) I. O.Troyanchuk, D. A. Efimov, N. V. Samsonenko, E. F. Shapovalova and H. Szymczak, *J. Phys.: Condens. Matter*, 1998, **10**, 7957–7966.

- (19) V. A. Khomchenko, I. O. Troyanchuk, A. I. Kurbakov, H. Gamari-Seale, V. V. Eremenko, H. Szymczak and R. Szymczak, *J. Magn. Magn.Mater.*, 2005, **288**, 224–235.
- (20) V. V. Krishnamurthy, I. Watanabe, K. Nagamine, H. Kuwahara and Y. Tokura, *Physica B*, 2000, **289-290**, 56-60.
- (21) A. M. Kadomtseva, Y. F. Popov, G. P. Vorobev, K. I. Kamilov, Y. S. Shtofich, A. A. Mukhin, V. Y. Ivanov and A. M. Balbashov,; *Physica B*, 2003, **329–333**, 854–855.
- (22) L.B. Duan, J.M. Liu, H.T. Zhu, W.C. Geng and H.Y. Xie, *Physica B*, 2011, **406**, 4682–4686.
- (23) I.O. Troyanchuk, *J. Magn. Magn.Mater.*, 2001, **231**, 53–56.
- (24) B. Samantaray, S.K. Srivastava and S. Ravi, *J. Magn. Magn.Mater.*, 2011, **323**, 2622–2626
- (25) Z.Q. Li, H. Liu, X.J. Liu, X.D. Liu, H.L. Bai, C.Q. Sun and E.Y. Jiang, *J. Magn. Magn. Mater.*, 2004, **284**, 133–139.
- (26) Y. K. Lakshmi and P. V. Reddy, *Phy. Lett. A*, 2011, **375**, 1543–1547.
- (27) B. Samantaray and S. Ravi, *J. Magn. Magn.Mater.*, 2009, **321**, 3671-3676.
- (28) B. Samantaray, S. Ravi and A. Perumal, *J. Magn.Magn.Mater.*, 2010, **322**, 3391–3395.
- (29) A. Nandy, A. Roychowdhury, D. Das and S.K. Pradhan, *Powder Technol.*, 2014, **254**, 538–547.
- (30) H.M. Rietveld, *Acta Crystallogr.*, 1967, **22**, 151–152.
- (31) H.M. Rietveld, *J. Appl. Crystallogr.*, 1969, **2**, 65–71.

- (32) L. Lutterotti, Maud Version 2.26. <http://www.ing.unitn.it/~maud/> (accessed 28.09.14)
- (33) L. Lutterotti, P. Scardi and P. Maistrelli, *J. Appl. Cryst.*, 1992, **25**, 459-462.
- (34) C. Shivakumara, M.S. Hegde, T. Srinivasa, N.Y. Vasanthacharya, G.N. Subbanna and N.P. Lalla, *J. Mater. Chem.*, 2001, **11**, 2572–2579.
- (35) R.D. Shannon, *Acta Cryst. A*, 1976, **32**, 751.
- (36) A. A. Mukhin, V. Y. Ivanov, V. D. Travkin and A. M. Balbashov, *J. Magn.Magn.Mater.*, 2001, **226-230**, 1139-1141.
- (37) C. Zener, *Phys. Rev.*, 1951, **82**, 403.